RSC Advances

PAPER

View Article Online
View Journal | View Issue

Cite this: *RSC Adv.*, 2023, **13**, 35562

Hydrophilic amorphous Cr_2O_3 supported Co species toward efficient hydrogen production from ammonia borane under visible light irradiation†

Fenglong Wu * and Jin Song *

Received 29th October 2023
Accepted 29th November 2023

DOI: 10.1039/d3ra07367j

rsc.li/rsc-advances

Herein, we synthesized a hydrophilic support formed from amorphous Cr_2O_3 and KIT-6 containing P123 using a simple solvent-free thermal method for Co species. The obtained catalyst (denoted as Co/Cr_2O_3-F-*X*) exhibits high activity for hydrogen production from ammonia borane (NH_3BH_3). The optimal Co/Cr_2O_3-F-0.5 exhibits the highest catalytic performance with the turnover frequency (TOF) value of 111.1 min^{-1}. Advanced characterizations suggest the high catalytic performance is attributed to the synergistic effect of the strong interaction between amorphous Cr_2O_3 and KIT-6 containing P123 and improved wettability of the catalyst.

1. Introduction

Hydrogen (H_2) as clean energy has attracted much attention owing to zero carbon emissions and high combustion value.[1–3] Ammonia borane (NH_3BH_3) as a promising hydrogen storage material with high hydrogen content (19.6 wt%) can present the solution for the challenges of safe transportation and storage of H_2.[4,5] The hydrolysis of NH_3BH_3 ($NH_3BH_3 + 2H_2O \rightarrow NH_4BO_2 + 3H_2$) is considered a promising strategy to generate H_2 due to the mild reaction conditions.[6,7] Supported heterogeneous catalysts play an important role in accelerating the reaction rate.[8–10] Various metal based catalysts including precious and non-precious metals have been employed for hydrolysis of NH_3BH_3.[11–18] However, the high cost of precious metals and low activity of non-precious metals hinder the large-scale application of NH_3BH_3. Many efforts have been made to decrease the dosage of precious metals and enhance the activity of non-precious metal based catalysts. Regulating the electronic structure of active metals is a common strategy to improve the activity of catalysts. Recently, introducing light irradiation into reaction systems, especially non-precious metals working as catalysts, has been proven to be an effective method to boost the charge imbalance distribution and then catalytic performance.[19–22] Nevertheless, the activity of non-precious metal catalyst is still far from satisfaction. As a result, it is urgent to rationally design the structure of non-noble metal catalysts to obtain high activity level.

Earth-abundant Co catalysts have been utilized in NH_3BH_3 hydrolysis.[23–26] For example, Co-Co_3O_4 has been employed as excellent catalyst for H_2 generation from NH_3BH_3 due to electronic structures at the interface and abundant adsorption site.[27] Our group have also prepared high performance Co/Cr_2O_3 composed of electron-deficient Co species and mesoporous Cr_2O_3. Cr_2O_3 is selected as support due to several reasons. Firstly, Cr_2O_3 has been widely applied in photoinduced reaction.[28] Secondly, Cr_2O_3 with relatively high work function induces electron transfer from Co. Importantly, electron-deficient Co species can decrease H_2O activation and dissociation energy barriers (rate-determining step in NH_3BH_3 hydrolysis) and then accelerate the rate of reaction.[29] To date, the design of catalyst has mainly focused on tuning electronic structures of active metal, while neglects catalyst wettability. The appropriate wettability of a catalyst can significantly enhance the adsorption and transfer of reactants, resulting in enhancement activity.[30] For example, Zhao group reported the activity of NiFe/NiFe:Pi toward oxygen evolution is significantly enhanced by tuning the wettability of the catalyst.[31] Xiao group reported the conversion of syngas to methane, dimethyl ether, and olefins can be regulated by controlling the catalyst hydrophobicity.[32] Accordingly, regulating catalyst wettability is an effective strategy to further boost the rate of NH_3BH_3 hydrolysis. Introduction of hydrophilic SiO_2 into reaction system can alter H_2O adsorption behaviour.[33] Therefore, introduction of material containing hydrophilic SiO_2 is effective strategy to enhance the catalyst activity.

Herein, we prepared hydrophilic Co-based catalyst Co/Cr_2O_3-F composed with amorphous Cr_2O_3 and functionalized with KIT-6 containing P123 and Co species based our group previous report. The optimal Co/Cr_2O_3-F-0.5 exhibits a high catalytic performance with TOF value of 111.1 min^{-1}. Advanced characterizations reveal the synergistic effect of strong interaction at interface and improved wettability is responsible for the high catalytic performance.

Department of Chemical and Environmental Engineering, Hetao College, Bayan Nur 015000, China. E-mail: wufenglong1983@126.com; jinsonght@sina.com

† Electronic supplementary information (ESI) available. See DOI: https://doi.org/10.1039/d3ra07367j

2. Experimental

2.1 Materials

Cobalt chloride hexahydrate ($CoCl_2 \cdot 6H_2O$), ammonia borane (NH_3BH_3), deuterium oxide (D_2O), potassium iodide (KI), tetraethyl orthosilicate ($C_8H_{20}O_4Si$) and sodium borohydride ($NaBH_4$) were obtained from Aladdin. Chromium(III) nitrate nonahydrate ($Cr(NO_3)_3 \cdot 6H_2O$) was obtained from Macklin. Isopropyl alcohol (C_3H_8O) was purchased from Tianjin Yongda ChemicalReagent Co. Ltd, poly(ethylene glycol)-*block*-poly(-propylene glycol)-*block*-poly(ethylene glycol) was obtained from Sigma-Aldrich. Potassium dichromate ($K_2Cr_2O_7$) were obtained from Sinopharm Chemical Reagent Co., Ltd.

2.2 Synthesis and photocatalytic H_2 production

Preparation of Cr_2O_3-F-0.5: KIT-6-F was firstly synthesized according to reported literature with minor modification.[34] We didn't calcine the sample to maintain the p123 in pore and on the surface of KIT-6. Next, a 0.5 g KIT-6-F and 0.2 g $Cr(NO_3)_3$ were ground and transferred into a Teflon-lined stainless steel and maintained at 240 °C for 3.5 h. Meanwhile, we prepared five other samples denoted as Cr_2O_3-F-*X* (*X* represents the quality of KIT-6-F). The KIT-6-E was prepared by calcination KIT-6-F at 550 °C for 3 h. The Cr_2O_3-E-0.5 was synthesized by KIT-6-E with same procedure as Cr_2O_3-F-0.5 for comparison.

Preparation of Co/Cr_2O_3-F-0.5 and catalytic H_2 production: 16.0 mg Cr_2O_3-F-0.5 was dispersed in containing 0.034 mmol $CoCl_2 \cdot 6H_2O$ aqueous solution (0.9 mL) for in reactor 1 h. Next, 0.068 mmol $NaBH_4$ acted as reduction and 1.71 mmol NH_3BH_3 were dissolved in 1.5 mL H_2O and was injected into the reactor. Meanwhile, the H_2 generated under visible light irradiation and in the dark. Five other samples including Co/Cr_2O_3-F-0.1, Co/Cr_2O_3-F-0.3, Co/Cr_2O_3-E-0.5, Co/KIT-6-F and Co/KIT-6-E were prepared by same method.

2.3 Catalyst characterization

Powder X-ray diffraction (PXRD) on D8 Advance with Cu-Kα radiation was employed to obtain crystalline structures and component of samples. Transmission electron microscopy (TEM, JEM-2100F) were used to observe the morphologies of samples. X-ray photoelectron spectroscopy (XPS) was conducted on a Thermo Scientific K-Alpha with pass energies = 50 eV and the calibrated using the C 1s peak at 284.8 eV was reference. PerkinElmer Lambda 750 was employed to collect UV-vis spectra of sample. Contact angle measurements were carried out on Dataphysics OCA40. TriStar II Plus 3.03 was used to measure the surface area of samples. The transient photocurrent and electrochemical impedance spectroscopy (EIS) were conducted on an electrochemical station (CHI600E) in 0.5 M Na_2SO_4 electrolyte. Fourier transform infrared (FTIR) was performed on FTIR-7600 spectrometer.

3. Results and discussion

3.1 Chemical structure analysis

As described in Fig. 1a, the catalyst Co/Cr_2O_3-F-0.5 was prepared by two-step method. Firstly, Cr_2O_3-F-0.5 was obtained by solvent-free thermal method. TEM image in Fig. 1b, S1a and S1b† shows the compound inherits the morphology of KIT-6. However, no long range ordered structure can be observed from HRTEM image, further confirming the amorphous nature of Cr_2O_3-F-0.5 (Fig. 1c). Moreover, the SAED of Cr_2O_3-F-0.5 (inset in Fig. 1c) demonstrates rings composed of diffraction spots, further verifying the amorphous feature of Cr_2O_3-F-0.5. XRD pattern displays abroad peak indexed to KIT-6,[35] and no characteristic peak assigned to Cr_2O_3 was clearly observed suggesting the sample is composed with KIT-6-F and amorphous Cr_2O_3 (Fig. 2). Additionally, samples including KIT-6-F, Cr_2O_3-F-0.1, Cr_2O_3-F-0.3, and Cr_2O_3-F-0.6 were also tested to further confirm the amorphous nature of support (Fig. 2). The result

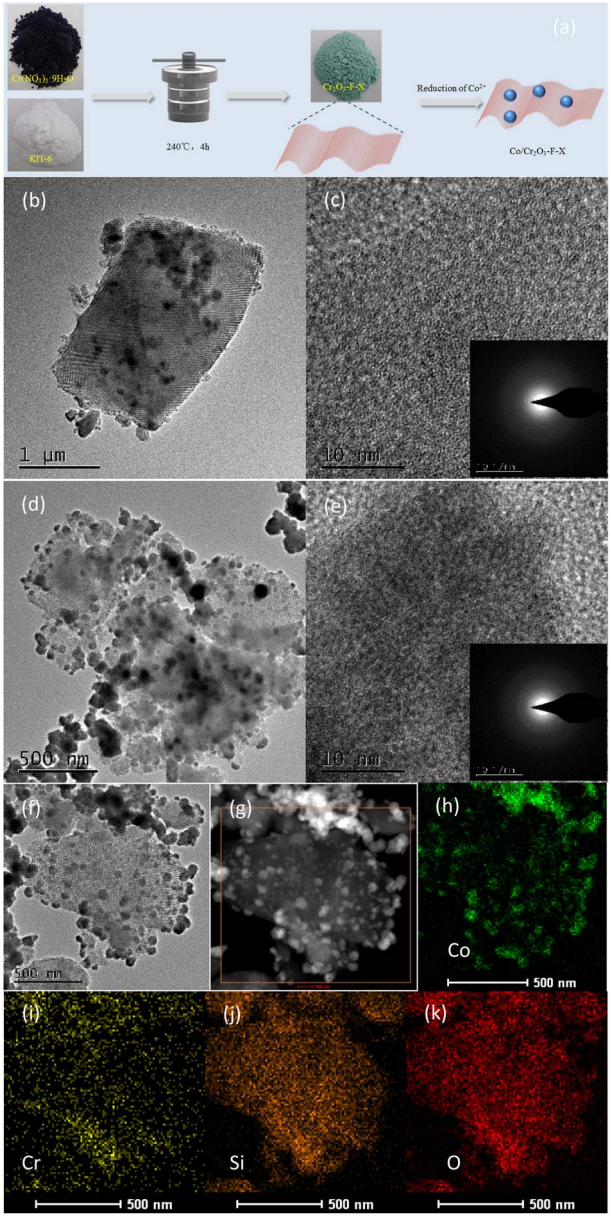

Fig. 1 (a) The illustration preparation process of Co/Cr_2O_3-F-0.5, (b and c) TEM images of Cr_2O_3-F-0.5 with different magnifications, (d–k) TEM images of Co/Cr_2O_3-F-0.5 with different magnifications, and the corresponding dark field elemental mappings.

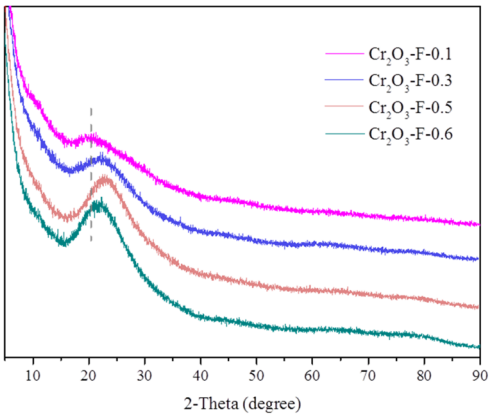

Fig. 2 XRD patterns of samples.

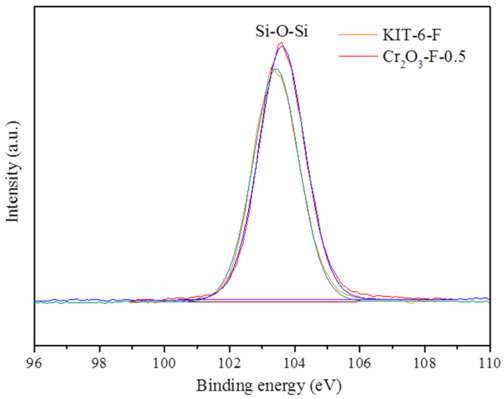

Fig. 3 XPS spectra of Si 2p in Cr_2O_3-F-0.5 and KIT-6-F.

shows the compound sample remains amorphous after adjusting the quality of KIT-6-F. Moreover, a closer look at the abroad peaks in the compound shifts to big larger 2θ angle with increasing KIT-6-F, suggesting the strong electronic interaction between KIT-6-F and Cr_2O_3. Similar phenomenon has been observed in metal alloys due to changed electronic structure.[36] Additionally, the image and structure of Cr_2O_3-E-0.5 also be tested for comparison. As shown in Fig. S2,† Cr_2O_3-E-0.5 displays the same morphology as KIT-6 and Cr_2O_3-F-0.5. XRD pattern shows an amorphous nature of Cr_2O_3-E-0.5 which is similar to the Cr_2O_3-F-0.5 (Fig. S3†). Therefore, the introduction of P123 cannot significantly affect the crystallinity of support. After loading Co species, TEM images from Fig. 1d and S4† show Co species are formed on the surface of Cr_2O_3-F-0.5. The long-range order also can't be observed in HRTEM image of Co/Cr_2O_3-F-0.5 in Fig. 1e, indicating the catalyst is composed of amorphous component. The SAED of Co/Cr_2O_3-F-0.5 (inset in Fig. 1e) further confirms the amorphous feature of catalyst. Additionally, the element mapping (Fig. 1f–k) and EDX further the Co species has supported on the surface of Cr_2O_3-F-0.5 (Fig. S5†). No obvious sharp peak assigned to Co is observed in XRD pattern of Co/Cr_2O_3-F-0.5 (Fig. S6†), suggesting the formation of amorphous Co species which is consistent with previous reports.[37] Additionally, the broad peak around 45° assigned to Co can further confirm the existence of amorphous Co.[38] BET surface area of Cr_2O_3-F-0.5 was calculated to be 246.2512 $m^2\ g^{-1}$ which is smaller than Co/Cr_2O_3-F-0.5 (296.8048 $m^2\ g^{-1}$) (Fig. S7 and S8†). The result suggests Co species mainly disperse on the surface of Cr_2O_3-F-0.5 rather than channel of KIT-6 maybe due to the interaction between Co^{2+} and amorphous Cr_2O_3.

XPS was employed to confirm the component Cr_2O_3-F-0.5 and complete XPS spectra for KIT-6-F for comparison. The full spectra display Si and O signal suggesting the coexisting of two elements in KIT-6-F. In addition to the aforementioned elemental signals, a faint Cr signal is also present in Cr_2O_3-F-0.5 (Fig. S9†), suggesting the compound is composed of Si, O and Cr elements. As shown in Fig. 3, in the high resolution XPS spectrum of Si 2p, a peak located at 103.5 eV assigns to the Si–O–Si band for KIT-6-F and Cr_2O_3-F-0.5.[39] Notably, high resolution XPS spectrum of Si 2p in Cr_2O_3-F-0.5 shifts to high binding energy compared with KIT-6-F. Similar phenomenon is observed in O 1s, suggesting the strong interaction between Cr_2O_3 and KIT-6-F (Fig. S10†). Additionally, high resolution XPS spectrum of Si in KIT-6-E and Cr_2O_3-E-0.5 also is collected to the effect of P123 on interaction between Cr_2O_3 and KIT-6. Compared to KIT-6-E, the Si 2p spectra in Cr_2O_3-E-0.5 undergo a shift to lower binding energy (Fig. S11†). This phenomenon is different from Cr_2O_3-F-0.5 due to the absence of P123.

FTIR spectra of KIT-6-F and Cr_2O_3-F-0.5 were collected to investigate the structure of samples and interaction. As shown in Fig. 4, the bands in two samples at around 1635, 1081, 960, 799 and 464 cm^{-1}correspond to absorbed water, symmetric stretching vibrations of Si–O–Si,–Si–OH vibration, asymmetric stretching vibrations of Si–O–Si, and bending vibrations of Si–O–Si, respectively.[40,41] Notably, compared with pristine KIT-6-F, the band at 1 635 960 and 464 cm^{-1} in compound are red-shifted, indicating the strong interaction between pristine KIT-6-F and Cr_2O_3, which is facilitated to regulate electron density of catalyst and obtain high performance.[42] Combined with the above characterization result, Cr_2O_3-F-0.5 strong interaction between amorphous Cr_2O_3 and KIT-6-F had been successfully synthesized. Additionally, The IR spectra of KIT-6-F were collected after five months (Fig. S12†). The result shows no

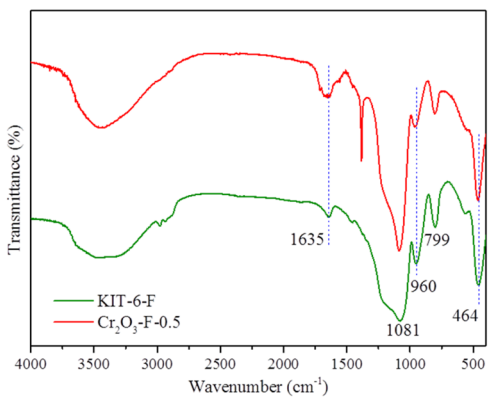

Fig. 4 IR spectra of Cr_2O_3-F-0.5 and KIT-6-F.

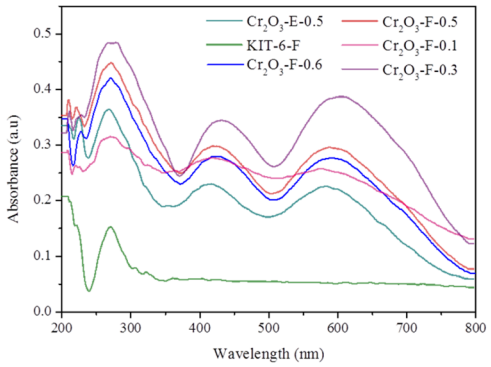

Fig. 5 UV-vis spectra of samples.

obvious change in characteristic peak is observed, suggesting reserved P123 on the surface of KIT-6 does not leach out.

UV-vis spectra were conducted to investigate the optical characterization of samples. As shown in Fig. 5, KIT-6-F is not capable of absorbing visible light while after coupling with Cr_2O_3, visible light absorption capacity is significantly improved and exhibits two absorbing peaks which is similar that of Cr_2O_3. Absorption strength is increasing with decreasing content of KIT-6-F because large quantities of KIT-6-F can form the light-shield effect and Cr_2O_3-F-0.3 has the strongest visible light reaction absorption. Notably, Cr_2O_3-F-0.1 doesn't show the best visible light response. This result may be due to too few KIT-6-F not beneficial to the formation of Cr_2O_3. Additionally, compared with Cr_2O_3-F-0.5, the Cr_2O_3-E-0.5 prepared by calcined KIT-6-F displays weak absorption of visible light, indicating the reserved p123 can strengthen the interaction between KIT-6-F and Cr_2O_3.

Separation efficiency of photogenerated electrons and holes has important influence in catalytic performance of catalyst. Transient photocurrent density was conducted to test the effect of reserved P123 on photogenerated carrier separation efficiency of compound. Cr_2O_3-E-0.5 also was test for comparison. As shown in Fig. 6a, the photogenerative carrier of the Cr_2O_3-E-0.5 can be effectively separated under visible light irradiation. In contrast, Cr_2O_3-F-0.5 exhibits stronger signal, revealing that Cr_2O_3-F-0.5 is benefit to carrier separation and transfer due to the strong interaction between KIT-6 and Cr_2O_3 with assistance of P123. EIS was performed to confirm the effect of different structure of samples on electron transition. As shown in Fig. 6b,

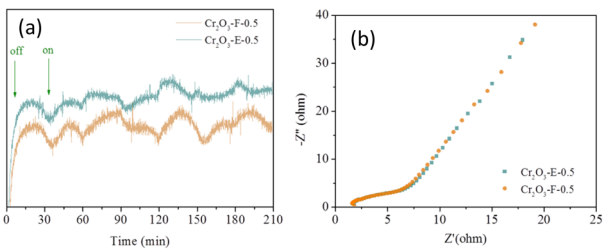

Fig. 6 (a) Profiles of time *versus* transient photocurrent density of two supports, (b) EIS Nyquist plots of samples.

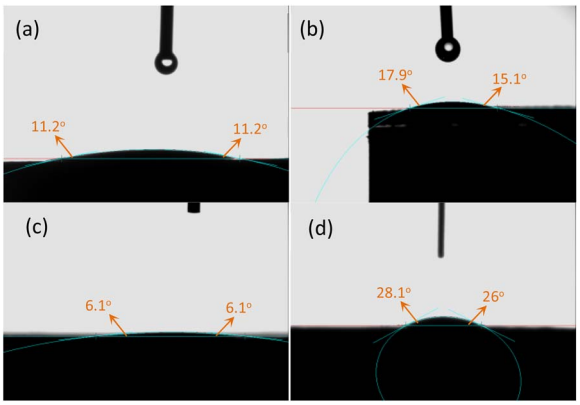

Fig. 7 Water contact angle measurements for (a) Cr_2O_3-F-0.5, (b) Cr_2O_3-E-0.5, (c) Co/Cr_2O_3-F-0.5 and (d) Co/Cr_2O_3-E-0.5.

Cr_2O_3-F-0.5 shows a slightly smaller arcradius, suggesting relatively small resistance to electron transport.

To investigate the effect of reserved P123 on wettability of support, contact angle measurements were conducted for Cr_2O_3-F-0.5, Cr_2O_3-E-0.5, Co/Cr_2O_3-F-0.5 and Co/Cr_2O_3-E-0.5. Generally speaking, the lower the contact angle is liable to better H_2O adsorption. As illustrated in Fig. 7, the Cr_2O_3-E-0.5 shows the water-droplet contact angle of 17.9° while contact angles of water droplet on the surface of the Cr_2O_3-F-0.5 decrease values with 11.2°, confirming reserved P123 can enhance the wettability of support and favour the charge transfer and accelerate the rate of NH_3BH_3 hydrolysis. The contact angles of water droplet on surface of Co/Cr_2O_3-E-0.5 (28.1°) is larger than Cr_2O_3-E-0.5. Conversely, the contact angles of water droplet on surface of Co/Cr_2O_3-F-0.5 (6.1°) is smaller than Cr_2O_3-F-0.5. The result suggests water can easily spread on the surface of Co/Cr_2O_3-F-0.5, leading to an increased H_2 evolution rate.

3.2 Photocatalytic performance

The photocatalytic activity of Co/Cr_2O_3-F-0.5 was tested in a reactor under visible light irradiation. Additionally, control experiments including Co/KIT-6-F, Co/Cr_2O_3-F-0.1, Co/Cr_2O_3-F-0.3, Co/Cr_2O_3-F-0.5, Co/Cr_2O_3-F-0.6, Co/Cr_2O_3-E-0.5 and Co/KIT-6-E were also conducted to reveal the origin of activity of catalyst. As shown in Fig. 8, both Co/KIT-6-F and Co/KIT-6-E exhibits similar activity in dark at same condition (Fig. 8a and b). Importantly, the activity of two catalysts is further boosted under visible irradiation (Fig. 8c and d). The enhanced catalytic performance is mainly attributed to the electronic structure changed induced by interband electron transfer of Co. In sharp contrast, the activity of Co/Cr_2O_3-F-0.5 exhibits greatly enhanced under visible irradiation than that of Co/KIT-6-F, while slightly boosted in dark. The TOF value of Co/Cr_2O_3-F-0.5 is 111.1 min^{-1} which is much higher than that of some tested non-precious metal based catalysts (Table 1). The enhanced performance is primarily attributed to the following aspects: firstly, introduction of Cr_2O_3 with high visible light utilization ratio induces the generation of photogenerative

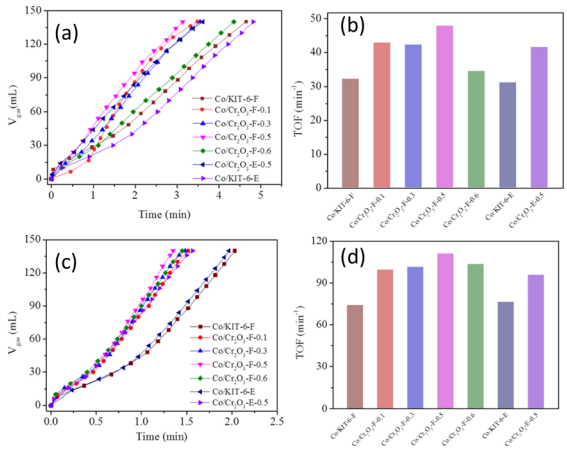

Fig. 8 Plots of time *versus* volume of H_2 evolution from NH_3BH_3 over Co-based catalysts (a) in dark, (b) corresponding TOF value (c) under visible light irradiation, (d) corresponding TOF value.

carriers to provide a greater drive for reaction progression. Secondly, the electron-deficiency degree of Co nanosheets is improved under visible irradiation, resulting in greatly decreased H_2O activation and dissociation energy barrier.[29] Thirdly, the increased NH_3BH_3 hydrolysis rate over Co/Cr_2O_3-E-0.5 under visible irradiation further conform the effect of Cr_2O_3 on activity of catalyst. Notably, the activity of Co/Cr_2O_3-E-0.5 with TOF 95.7 min^{-1} is lower than Co/Cr_2O_3-F-0.5. Combined with the UV-vis, EIS, transient photocurrent density and water contact angle measurements experimental result, the reserved P123 on surface of KIT-6 not only construct strong interaction among multiple interfaces but also improve catalyst wettability, which is benefit to adsorption of reactant molecules and carrier transfer and accelerate the NH_3BH_3 hydrolysis rate. Additionally, we added a control experiment over Co supported on Cr_2O_3-F-0.5-M (physically mixed KIT-6-F and Cr_2O_3) to provide evidence for the effect of strong interaction between KIT-6-F and Cr_2O_3 on Co-based catalytic activity. As expected, the performance of Co/Cr_2O_3-F-0.5-M with TOF of 76.9 min^{-1} is greatly reduced in comparison to Co/Cr_2O_3-F-0.5 (Fig. S13†). Therefore, the synergistic effect of high visible light utilization, strong interaction between KIT-6-F and Cr_2O_3 and improved wettability leads to a significant enhanced catalyst performance under visible irradiation.

In order to reveal the influence of interface effect on catalyst performance, the control experiments were performed based on Co/Cr_2O_3-F-0.1, Co/Cr_2O_3-F-0.3, Co/Cr_2O_3-F-0.5, Co/Cr_2O_3-F-0.6. It can be clearly observed that the introduction of amorphous Cr_2O_3 in support can slightly boost the activity of Co-based catalyst in dark (Fig. 8c). However, the activity of catalyst containing KIT-6-F can significantly improve under visible irradiation. Moreover, the activity enhances with increased KIT-6-F mass and the catalyst Co/Cr_2O_3-F-0.5 exhibits highest performance. The activity decreases when the mass of KIT-6-F in support is continued to increase due to light-shield effect.

Photogenerated carriers can not only tune the electronic structure of catalyst but also induce the generation of radical intermediates such as hydroxyl radicals (˙OH), which have significantly effect on the performance of catalyst in light induced reaction. Therefore, we investigated the influence of ˙OH to the performance of Co/Cr_2O_3-F-0.5 using trapping experiment and EPR characterization. In capture experiment, electrons, holes and ˙OH was captured by $K_2Cr_2O_7$ (100 μM), KI(100 μM) and 2-propanol (IPA) (100 μL), respectively.[47] The result was shown in Fig. 9a and b, the adding of sacrificial agents in reaction system can decrease the hydrolysis rate of NH_3BH_3, suggesting the photogenerated carriers and radical intermediates can boost the activity of Co/Cr_2O_3-F-0.5. It is worth noting that the effect of photogenerated carriers and radical intermediates on enhanced activity is different based on different catalyst. ESR measurements was conducted to confirm the existing of ˙OH and superoxide anions ($˙O_2^-$) originated from the reaction of dissolved O_2 and photogenerated electron was also measured which can improve the rate of NH_3BH_3 hydrolysis.[46] As shown in Fig. 9c, no characteristic signal of ˙OH is observed in the dark based on Cr_2O_3-F-0.5, but the signal with 1 : 2 : 2 : 1 strength appears under irradiation. The same phenomenon is observed in $˙O_2^-$ detection (Fig. 9d). These results further conform the existing of ˙OH and $˙O_2^-$ under light irradiation.

Table 1 Activities of catalysts in the H_2 evolution from NH_3BH_3

Catalyst	TOF (min^{-1})	References	Temperature (K)	Irradiation
Co/Cr_2O_3-F-0.3	101.4	This work	298	With
Co/Cr_2O_3-F-0.5	111.1	This work	298	With
Co/Cr_2O_3-F-0.6	103.4	This work	298	With
Co/Cr_2O_3	106.8	29	298	With
NiCo-NC	35.2	43	298	Without
Co_3O_4–SnO_2	17.6	44	298	Without
Ni/Ni_2P	68.3	4	298	Without
Co@N-C-700	5.6	23	298	With
NiCu/CNS	30.6	22	298	With
$NiCu/SiO_2$	25.3	45	298	Without
$Cu_{0.5}Co_{0.5}O$-rGO	81.7	24	room	Without
Cu/MIL-101	28.22	46	298	With

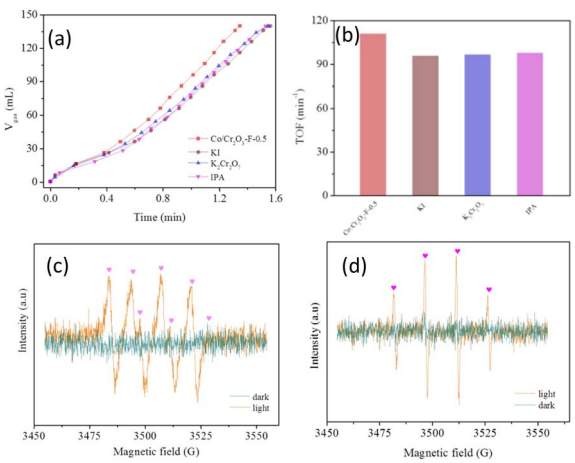

Fig. 9 (a) and (b) Role of hydroxyl radicals and superoxide anions in NH_3BH_3 hydrolysis underlight irradiation. (c) and (d) DMPO ESR spin-labeling for $˙O_2^-$ and ˙OH.

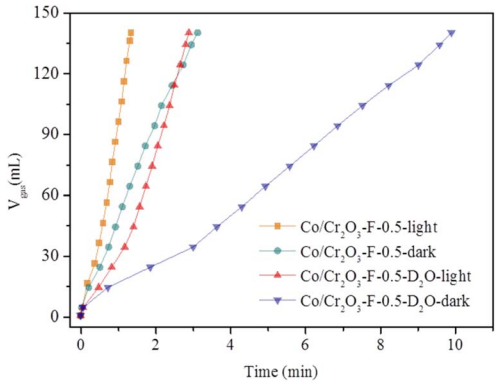

Fig. 10 Plots of time *versus* volume of hydrogen evolution from NH_3BH_3 in H_2O or D_2O over Co/Cr_2O_3-F-0.5 under visible light irradiation and in dark.

The cleavage of O–H bond in H_2O molecules is the rate-determining step in NH_3BH_3 hydrolysis.[48,49] To further confirm the conclusion, the kinetic isotope effect (KIE: KH/KD) is conducted. As shown in Fig. 10 the H_2 evolution rates greatly decreases using D_2O to replace H_2O both light irradiation and in dark. The value of KIE is 2.89 in darkness and is 2.13 under light irradiation. This result indicates the cleavage of O–H bond is the rate-determining step over Co/Cr_2O_3-F-0.5 toward the hydrolysis of NH_3BH_3.

According to characterization, experimental results and previous report, we propose a possible mechanism for NH_3BH_3 hydrolysis induced by visible light. Firstly, Co species and Cr_2O_3-F-0.5 absorbs visible light. Secondly, photoinduced electrons and holes are generated and transfer to the surface of Co species and Cr_2O_3-F-0.5. Meanwhile, photoinduced electrons transfer from active species to support then $^{\bullet}OH$ and $^{\bullet}O_2^-$ are formed in this process. Thirdly, the B–H bond in NH_3BH_3 and O–H bond in H_2O are broken and H_2 is generated. $^{\bullet}OH$ and $^{\bullet}O_2^-$ can accelerate the breaking of two kinds of bonds. Notably, the strong interaction among multicomponent and enhanced wettability can favor the transition of photoinduced carriers, $^{\bullet}OH$ and $^{\bullet}O_2^-$ and then improve the production rate of H_2.

4. Conclusions

We synthesized a hydrophilic support by simple solvent-free thermal method. The compound works as amazing support for Co species. The optimal Co/Cr_2O_3-F-0.5 exhibits a highest catalytic performance for hydrogen production from NH_3BH_3 with TOF value of 111.1 min^{-1}. XRD, IR and XPS results indicate strong interaction between KIT-6-F and Cr_2O_3-F. Contact angle measurement verifies Cr_2O_3-F-0.5 has improved wettability. The synergistic effect of strong interaction and improved wettability induces high catalytic performance of Co/Cr_2O_3-F-0.5.

Conflicts of interest

There are no conflicts to declare.

Acknowledgements

The authors gratefully acknowledge the financial support from the National Natural Science Foundation of China (52161038), Young Talents of Science and Technology in Universities of Inner Mongolia Autonomous Region (NJYT23033), Natural Science Foundation of Inner Mongolia Autonomous Region (2022MS05012), and the Talent Development Fund Project of Inner Mongolia Autonomous Region ([2022]-110).

References

1 N. Dubouis, A. Serva, R. Berthin, G. Jeanmairet, B. Porcheron, E. Salager, M. Salanne and A. Grimaud, *Nat. Catal.*, 2020, **3**, 656–663.
2 J. He, Z. Huang, W. Che, X. Xiao, Z. Yao, Z. Liang, L. Zhan, L. Lv, J. Qi, X. Fan and L. Chen, *Chem. Eng. J.*, 2022, **431**, 133697.
3 M. K. Sarmah, T. P. Singh, P. Kalita and A. Dewan, *RSC Adv.*, 2023, **13**, 25253–25275.
4 Y. Lin, L. Yang, H. Jiang, Y. Zhang, D. Cao, C. Wu, G. Zhang, J. Jiang and L. Song, *J. Phys. Chem. Lett.*, 2019, **10**, 1048–1054.
5 Y. Meng, Q. Sun, T. Zhang, J. Zhang, Z. Dong, Y. Ma, Z. Wu, H. Wang, X. Bao, Q. Sun and J. Yu, *J. Am. Chem. Soc.*, 2023, **145**, 5486–5495.
6 L. Wei, Y. Lu, R. Lua and Y. Cui, *RSC Adv.*, 2023, **13**, 7614–7620.
7 C. Wang, J. Tuninetti, Z. Wang, C. Zhang, R. Ciganda, L. Salmon, S. Moya, J. Ruiz and D. Astruc, *J. Am. Chem. Soc.*, 2017, **139**, 11610–11615.
8 C. D. Mboyi, D. Poinsot, J. Roger, K. Fajerwerg, M. L. Kahn and J.-C. Hierso, *Small*, 2021, **17**, 2102759.
9 H. Wu, Y. Chen, Y. Fan, X. Lu, L. Li, B. Liu, B. Li and S. Lu, *Int. J. Hydrogen Energy*, 2020, **45**, 30325–30340.
10 S. Guan, Y. Liu, H. Zhang, R. Shen, H. Wen, N. Kang, J. Zhou, B. Liu, Y. Fan, J. Jiang and B. Li, *Adv. Sci.*, 2023, **10**, 2300726.
11 Y. Ren, J. Duan, X. Liu, L. Bian, Y. Fan and B. Liu, *Energy Fuels*, 2021, **35**, 16222–16231.
12 S. Akbayrak and S. Özkar, *J. Colloid Interface Sci.*, 2021, **596**, 100–107.
13 L.-T. Guo, Y.-Y. Cai, J.-M. Ge, Y.-N. Zhang, L.-H. Gong, X.-H. Li, K.-X. Wang, Q.-Z. Ren, J. Su and J.-S. Chen, *ACS Catal.*, 2015, **5**, 388–392.
14 W. Chen, G. Lv, J. Fu, H. Ren, J. Shen, J. Cao and X. Liu, *ACS Appl. Mater. Interfaces*, 2021, **13**, 50017–50026.
15 B. Wang, L. Xiong, H. Hao, H. Cai, P. Gao, F. Liu, X. Yu, C. Wu and S. Yang, *J. Alloys Compd.*, 2020, **844**, 156253.
16 J. Liao, Y. Wu, Y. Shao, Y. Feng, X. Zhang, W. Zhang, J. Li, M. Wu, H. Dong, Q. Liu and H. Li, *Chem. Eng. J.*, 2022, **449**, 137755.
17 F. Qiu, X. Hao, W. Huang, Y. Wu, R. Chu, J. Yang, W. Fu, G. Ren, C. Xu and W. Bao, *RSC Adv.*, 2023, **13**, 632–637.
18 L. Zhang, J. Ye, Y. Tu, Q. Wang, H. Pan, L. Wu, X. Zheng and J. Zhu, *Nano Res.*, 2022, **15**, 3034–3041.
19 H. Yin, Y. Kuwahara, K. Mori and H. Yamashita, *J. Mater. Chem. A*, 2018, **6**, 10932–10938.

20 N. Kang, Q. Wang, R. Djeda, W. Wang, F. Fu, M. M. Moro, M. de los A. Ramirez, S. Moya, E. Coy, L. Salmon, J.-L. Pozzo and D. Astruc, *ACS Appl. Mater. Interfaces*, 2020, **12**, 53816–53826.
21 N. Kang, X. Wei, R. Shen, B. Li, E. G. Cal, S. Moya, L. Salmon, C. Wang, E. Coy, M. Berlande, J.-L. Pozzo and D. Astruc, *Appl. Catal., B*, 2023, **320**, 121957.
22 S. Zhang, M. Li, L. Li, F. Dushimimana, J. Zhao, S. Wang, J. Han, X. Zhu, X. Liu, Q. Ge and H. Wang, *ACS Catal.*, 2020, **10**, 14903–14915.
23 H. Wang, Y. Zhao, F. Cheng, Z. Tao and J. Chen, *Catal. Sci. Technol.*, 2016, **6**, 3443–3448.
24 H. Zheng, K. Feng, Y. Shang, Z. Kang, X. Sun and J. Zhong, *Inorg. Chem. Front.*, 2018, **5**, 1180–1187.
25 H. Zhang, X. Gu, P. Liu, J. Song, J. Cheng and H. Su, *J. Mater. Chem. A*, 2017, **5**, 2288–2296.
26 J. Song, X. Gu, Y. Cao and H. Zhang, *J. Mater. Chem. A*, 2019, **7**, 10543–10551.
27 H. Wu, M. Wu, B. Wang, X. Yong, Y. Liu, B. Li, B. Liu and S. Lu, *J. Energy Chem.*, 2020, **48**, 43–53.
28 Y. Chen, G. Mao, Y. Tang, H. Wu, G. Wang, L. Zhang and Q. Liu, *Chin. J. Catal.*, 2021, **42**, 225–234.
29 J. Song and F. Wu, *Nanoscale*, 2023, **15**, 16741–16751.
30 L. Wang and F.-S. Xiao, *ChemCatChem*, 2014, **6**, 3048–3052.
31 Y. Li and C. Zhao, *ACS Catal.*, 2017, **7**, 2535–2541.
32 C. Wang, L. Liu, H. Li, L. Wang and F.-S. Xiao, *Matter*, 2023, **6**, 2697–2710.
33 X. Zhang, Y. Zhao, X. Jia, Y. Zhao, L. Shang, Q. Wang, G. I. N. Waterhouse, L.-Z. Wu, C.-H. Tung and T. Zhang, *Adv. Energy Mater.*, 2018, **8**, 1702780.
34 K. Soni, B. S. Rana, A. K. Sinha, A. Bhaumik, M. Nandi, M. Kumar and G. M. Dhar, *Appl. Catal., B*, 2009, **90**, 55–63.
35 H. Al-shaikh, J. Lasri, J. G. Knight and S. T. Al-Goul, *Fuel*, 2022, **325**, 124962.
36 P. Liu, X. Gu, H. Zhang, J. Cheng, J. Song and H. Su, *Appl. Catal., B*, 2017, **204**, 497–504.
37 J. Song, F. Wu, H. Ma, Y. Liu, N. Song, J. Yu and Y. Wang, *ACS Appl. Energy Mater.*, 2021, **4**, 8377–8385.
38 J. Pang, S. Jin, J. Hou, G. Wang, K. Sun, Y. Zheng, H. Li, Y. Shen, X. Yang and L. Chen, *Sens. Actuators, B*, 2023, **374**, 132725.
39 Y. Ding, J. Wang, M. Liao, J. Li, L. Zhang, J. Guo and H. Wu, *Chem. Eng. J.*, 2021, **418**, 129470.
40 P. Han, T. Liu, X. Ji and S. Tang, *Chin. Chem. Lett.*, 2018, **29**, 1305–1309.
41 X. Zhou, H. Zhao, S. Liu, D. Ye, R. Qu, C. Zheng and X. Gao, *Appl. Surf. Sci.*, 2020, **525**, 146382.
42 P. Zhou, S.-X. Guo, L. Li, T. Ueda, Y. Nishiwaki, L. Huang, Z. Zhang and J. Zhang, *Angew. Chem., Int. Ed.*, 2023, **62**, e202214881.
43 L. Zhao, Q. Wei, L. Zhang, Y. Zhao and B. Zhang, *Renewable Energy*, 2021, **173**, 273–282.
44 H.-Z. Wang, Y.-X. Shao, Y.-F. Feng, Y.-J. Tan, Q.-Y. Liao, X.-D. Chen, X.-F. Zhang, Z.-H. Guo and H. Li, *Rare Met.*, 2023, **42**, 3013–3023.
45 K. Guo, Y. Ding, J. Luo, M. Gu and Z. Yu, *ACS Appl. Energy Mater.*, 2019, **2**, 5851–5861.
46 M. Wen, Y. Cui, Y. Kuwahara, K. Mori and H. Yamashita, *ACS Appl. Mater. Interfaces*, 2016, **8**, 21278–21284.
47 S. Jo, P. Verma, Y. Kuwahara, K. Mori, W. Choi and H. Yamashita, *J. Mater. Chem. A*, 2017, **5**, 21883–21892.
48 S. Zhou, Y. Yang, P. Yin, Z. Ren, L. Wang and M. Wei, *ACS Appl. Mater. Interfaces*, 2022, **14**, 5275–5286.
49 Z. Li, T. He, L. Liu, W. Chen, M. Zhang, G. Wu and P. Chen, *Chem. Sci.*, 2017, **8**, 781–788.